Available online at www.sciencedirect.com
ScienceDirect
Geochimica et Cosmochimica Acta 75 (2011) 5540–5558
Geochimica et Cosmochimica Acta
www.elsevier.com/locate/gca

A quantitative reconstruction of organic matter and nutrient diagenesis in Mediterranean Sea sediments over the Holocene

Daniel C. Reed *, Caroline P. Slomp, Gert J. de Lange

Department of Earth Sciences (Geochemistry), Faculty of Geosciences, Utrecht University, P.O. Box 80.021, 3508 TA Utrecht, The Netherlands

Received 19 November 2010; accepted in revised form 29 June 2011; available online 14 July 2011

Abstract

A multicomponent diagenetic model was developed and applied to reconstruct the conditions under which the most recent sapropel, S1, was deposited in the eastern Mediterranean Sea. Simulations demonstrate that bottom waters must have been anoxic and sulphidic during the formation of S1 and that organic matter deposition was approximately three times higher than at present. Nevertheless, most present day sediment and pore water profiles — with the exception of pyrite, iron oxyhydroxides, iron-bound phosphorus and phosphate — can be reproduced under a wide range of redox conditions during formation of S1 by varying the depositional flux of organic carbon. As a result, paleoredox indicators (e.g., C_{org}:S ratio, C_{org}:P_{org} ratio, trace metals) are needed when assessing the contribution of oxygen-depletion and enhanced primary production to the formation of organic-rich layers in the geological record. Furthermore, simulations show that the organic carbon concentration in sediments is a direct proxy for export production under anoxic bottom waters.

The model is also used to examine the post-depositional alteration of the organic-rich layer focussing on nitrogen, phosphorus, and organic carbon dynamics. After sapropel formation, remineralisation is dominated by aerobic respiration at a rate that is inversely proportional to the time since bottom waters became oxic once again. A sensitivity analysis was undertaken to identify the most pertinent parameters in regulating the oxidation of sapropels, demonstrating that variations in sedimentation rate, depositional flux of organic carbon during sapropel formation, bottom water oxygen concentration, and porosity have the largest impact. Simulations reveal that sedimentary nutrient cycling was markedly different during the formation of S1, as well as after reoxygenation of bottom waters. Accumulation of organic nitrogen in sediments doubled during sapropel deposition, representing a significant nitrogen sink. Following reventilation of deep waters, N_2 production by denitrification was almost 12 times greater than present day values. Phosphorus cycling also exhibits a strong redox sensitivity. The benthic efflux of phosphate was up to 3.5 times higher during the formation of S1 than at present due to elevated depositional fluxes of organic matter coupled with enhanced remineralisation of organic phosphorus. Reoxygenation of bottom waters leads to a large phosphate pulse to the water column that declines rapidly with time due to rapid oxidation of organic material. The oxidation of pyrite at the redox front forms iron oxyhydroxides that bind phosphorus and, thus, attenuate the benthic phosphate efflux. These results underscore the contrasting effects of oxygen-depletion on sedimentary nitrogen and phosphorus cycling. The simulations also confirm that the current conceptual paradigm of sapropel formation and oxidation is valid and quantitatively coherent.

* Corresponding author.
E-mail address: d.reed@geo.uu.nl (D.C. Reed).

0016-7037/$ - see front matter © 2011 Elsevier Ltd. All rights reserved.
doi:10.1016/j.gca.2011.07.002

1. INTRODUCTION

Burial of organic carbon and pyrite in marine sediments ultimately regulates atmospheric oxygen and carbon dioxide concentrations on geological time-scales (Holland, 1984; Berner, 1999). Global oxygen and carbon cycles can be perturbed by the episodic deposition of organic-rich sediments associated with periods of oxygen-depletion in bottom waters. Throughout the world, hypoxic regions have grown exponentially in recent decades (Diaz and Rosenburg, 2008), affecting not only oxygen and carbon cycling but also nutrient dynamics. Under low oxygen conditions, sedimentary nutrient retention is not simply a function of organic carbon preservation; for example, phosphorus binds to iron oxyhydroxides, which are redox-sensitive (Slomp et al., 1996), and organic phosphorus is remineralised faster than organic carbon (Ingall and Jahnke, 1994; Slomp et al., 2002). The impact of organic-rich layers on biogeochemical processes provides impetus for identifying and quantifying the mechanisms responsible for their formation and post-depositional alteration, particularly with regard to nutrient dynamics.

Sediments underlying the Mediterranean Sea are composed of organic-poor deposits interspersed with organic-rich layers, commonly termed *sapropels* (Kidd et al., 1978). Presently, oligotrophic surface waters provide a modest flux of organic carbon to the sediment, most of which escapes burial due to rapid decomposition under oxic conditions (Van Santvoort et al., 2002). In contrast, sapropels are indicative of periods of elevated productivity and enhanced organic matter preservation due to anoxic bottom waters (Thomson et al., 1999; de Lange et al., 2008). These conditions arose due to an increased input of nutrient-bearing freshwater into the Mediterranean Sea as a result of higher precipitation in the catchment area (Rohling and Hilgen, 1991). Greater stratification retarded mixing in the water column and reduced ventilation of deep waters, while an intensified rain of organic matter from the euphotic zone increased oxygen consumption at depth leading to anoxic bottom waters. Consequently, organic-rich layers were formed and persisted as a result of the relatively slow kinetics of sulphate reduction and a dearth of other oxidants (de Lange et al., 1994; Moodley et al., 2005). Upon reoxygenation of bottom waters, sapropels were subject to aerobic oxidation, which attenuates the amount of carbon that is ultimately buried. The downward post-depositional oxidation of these organic-rich layers, or *burn-down*, varies widely between sites and with sediment age, from well-preserved sapropels to those that have been entirely remineralised. The extent that various factors regulate burn-down remains poorly quantified.

Analysis of sapropels not only aids the palaeoreconstruction of the Mediterranean Sea, but also provides insight into the long-term dynamics of sediment biogeochemistry subject to transient redox conditions. Here, we develop a diagenetic model that provides a comprehensive view of the system by incorporating all relevant chemical components, transport processes, and reactions, as opposed to focussing on an individual proxy or process. The initial goal of the model is to verify that the current conceptualisation of sapropel formation and oxidation is indeed *quantitatively* coherent, which is achieved by comparing model output and published pore water and sediment data. Furthermore, since the vast majority of model parameters are known either from the modelled dataset (i.e., Slomp et al., 2002) or from other literature (e.g., Basso et al., 2004), any parameters that cannot be measured directly can be inferred by fitting the model to observed sediment profiles. Following successful groundtruthing, a sensitivity analysis is undertaken to examine the influence that various environmental parameters exert on the preservation and remineralisation of sapropels. Next, the contributions of redox conditions and productivity to the formation and persistence of organic-rich deposits are considered. Finally, the model is used to explore organic matter, nitrogen, and phosphorus dynamics during the deposition and subsequent oxidation of the sapropel.

2. MODEL FORMULATION

2.1. General form

The model describes the mass balance of dissolved and particulate chemical species in a 1D sediment column (Berner, 1980). A total of 22 different chemical species are considered (Table 1), which are subject to various transport processes and reactions. Both solutes and solids are buried by sedimentation and displaced by bioturbation within the mixed layer (i.e., the region inhabited by benthic fauna in the vicinity of the sediment–water interface). In addition, dissolved species are also transported by molecular diffusion. Bioirrigation is omitted here due to faunal considerations discussed in Section 3.1. The components also interact with one another through a suite of reactions taken from Boudreau (1996), Wang and Van Cappellen (1996), Berg et al. (2003) and Rickard (1997) (Table 2). The model takes the form of a system of partial differential equations (PDEs) that, when solved, furnish the vertical distributions of the components as a function of time.

The origin of the reference frame is tied to the sediment–water interface and deposition therefore results in a downward advective flux with a velocity equal to the accumulation rate (Berner, 1980; Boudreau, 1997). Advection is constant throughout the model domain as there is no compaction and a constant porosity. Bioturbation, the mixing of sediment particles by animals (Richter, 1952), appears in the model as a diffusive term, often referred to as *biodiffusion* (Goldberg and Koide, 1962; Guinasso and Schink, 1975). The intensity of biogenic sediment reworking is assumed to decay exponentially with depth, representing the decline in macroinfaunal density with increasing distance from the sediment–water interface (e.g., Boudreau, 1986). The mathematical details of the model are given in Appendix A.

2.2. Reaction kinetics

Reactions considered by the model are divided into two groups: primary redox reactions and other reactions (Table 2). Primary redox reactions describe the degradation

Table 1
Chemical species included in the diagenetic model.

Species	Notation	Type
Organic carbon type[a] *i*	C^{i}_{org}	Solid
Organic nitrogen type *i*	N^{i}_{org}	Solid
Organic phosphorus type *i*	P^{i}_{org}	Solid
Oxygen	O_2	Solute
Nitrate	NO_3^-	Solute
Manganese oxyhydroxides	MnO_2	Solid
Iron oxyhydroxides	$Fe(OH)_3$	Solid
Sulphate	$SO_4^=$	Solute
Manganese	Mn^{2+}	Solute
Iron	Fe^{2+}	Solute
Ammonia/ammonium[b]	ΣNH_4^+	Solute
Phosphate[b]	$\Sigma H_2PO_4^-$	Solute
Hydrogen sulphide[b]	ΣH_2S	Solute
Methane	CH_4	Solute
Elemental sulphur	S_0	Solid
Iron monosulphide	FeS	Solid
Pyrite	FeS_2	Solid
Iron-bound phosphorus	Fe-P	Adsorbed/coprecipitated
Authigenic phosphorus	Auth-P	Solid

[a] There are two types of organic species: reactive (α) and refractory (β).
[b] Σ denotes that all species of an acid are included (e.g., $\Sigma NH_4^+ = NH_3 + NH_4^+$).

of organic matter by a variety of oxidants and are typically assumed to conform to Monod or Blackman kinetics, or a combination of the two (e.g., Boudreau, 1996; Wang and Van Cappellen, 1996; Berg et al., 2003). Such schemes replicate the observed succession of oxidants (i.e., Froelich et al., 1979) by shutting down pathways when an oxidant is exhausted and inhibiting pathways in the presence of oxidants with higher metabolic free energy yields. Oxidants included in the model are (in descending order of energy yield) O_2, NO_3^-, Mn-oxyhydroxides, Fe-oxyhydroxides, and $SO_4^=$. In the absence of these species, remineralisation occurs through methanogenesis, whereby organic matter adopts the role of both the electron acceptor and donor. In this model, the succession of oxidants during organic matter decomposition is described by means of Monod kinetics (Appendix B, Table B1). An attenuation factor, Ψ, is used to retard organic matter degradation by means of sulphate reduction and methanogenesis, since these remineralisation pathways progress more slowly than others (Moodley et al., 2005).

There are six different organic pools in the model: reactive and refractory species of organic carbon, nitrogen and phosphorus. Reactive pools are subject to remineralisation, while the refractory pools are entirely inert. Organic carbon, nitrogen, and phosphorus are treated separately to allow for dynamic C:N:P ratios in time and space. In particular, organic matter deposited during and after sapropel formation differs in composition, while organic phosphorus is remineralised faster than organic carbon and nitrogen under oxygen-depleted bottom waters (Ingall et al., 1993; Ingall and Jahnke, 1994; Slomp et al., 2002). The remineralisation rate of organic nitrogen (R^{α}_{Norg}), that is, the rate at which labile organic nitrogen is lost and ammonia produced, is calculated from the organic carbon remineralisation rate (R^{α}_{Corg}) and the C:N ratio:

$$R^{\alpha}_{Norg} = R^{\alpha}_{Corg}\frac{[N^{\alpha}_{org}]}{[C^{\alpha}_{org}]} \quad (1)$$

where $[N^{\alpha}_{org}]$ and $[C^{\alpha}_{org}]$ are the concentration of labile organic nitrogen and carbon, respectively. Regeneration of organic phosphorus (R^{α}_{Porg}) and release of phosphate are treated in a similar fashion, although under anoxic conditions the organic phosphorus remineralisation rate is enhanced by a factor, ε. Therefore,

$$R^{\alpha}_{Porg} = \varepsilon R^{\alpha}_{Corg}\frac{[P^{\alpha}_{org}]}{[C^{\alpha}_{org}]} \quad (2)$$

where $[P^{\alpha}_{org}]$ is the concentrations of labile organic phosphorus. That is to say, $\varepsilon > 1$ for sulphate reduction and methanogenesis to simulate faster remineralisation of organic phosphorus relative to organic carbon (e.g., Ingall and Jahnke, 1994; Slomp et al., 2002) and $\varepsilon = 1$ for all other remineralisation pathways. ε is constrained by fitting model generated profiles for phosphate and organic phosphorus to observations.

All other reactions — with the exception of sulphur disproportionation (R19) — are second order and taken from Boudreau (1996), Wang and Van Cappellen (1996), Berg et al. (2003) or Rickard (1997) (Appendix B, Table B2).

2.3. Model solution

To solve the model, two boundary conditions are needed for each species. That is to say, the behaviour of every solute and solid must be specified at both the sediment–water interface and base of the model domain. For particulate components, a depositional flux is prescribed at the sediment–water interface and material is lost at the lower boundary by burial. For solutes, bottom water concentrations are given at the upper boundary,

Table 2
Chemical reactions included in the diagenetic model. Note that Fe-P represents $H_2PO_4^-$ that is bound to iron oxyhydroxides.

Primary redox reactions[a]

$$OM + aO_2 \rightarrow aCO_2 + bNH_3 + cH_3PO_4 + aH_2O \quad (R1)$$

$$OM + \frac{4a}{5}NO_3^- + \frac{4a}{5}H^+ \rightarrow aCO_2 + bNH_3 + cH_3PO_4 + \frac{2a}{5}N_2 + \frac{7a}{5}H_2O \quad (R2)$$

$$OM + 2aMnO_2 + 4aH^+ \rightarrow aCO_2 + bNH_3 + cH_3PO_4 + 2aMn^{2+} + 3aH_2O \quad (R3)$$

$$OM + 4aFe(OH)_3 + 4a\chi Fe\text{-}P + 12aH^+ \rightarrow aCO_2 + bNH_3 + (c + 4a\chi)H_3PO_4 + 4aFe^{2+} + 13aH_2O \quad (R4)$$

$$OM + \frac{a}{2}SO_4^{=} + aH^+ \rightarrow aCO_2 + bNH_3 + cH_3PO_4 + \frac{a}{2}H_2S + aH_2O \quad (R5)$$

$$OM \rightarrow \frac{a}{2}CO_2 + bNH_3 + cH_3PO_4 + \frac{a}{2}CH_4 \quad (R6)$$

Other reactions[b]

$$2O_2 + NH_4^+ + 2HCO_3^- \rightarrow NO_3^- + 2CO_2 + 3H_2O \quad (R7)$$

$$O_2 + 2Mn^{2+} + 4HCO_3^- \rightarrow 2MnO_2 + 4CO_2 + 2H_2O \quad (R8)$$

$$O_2 + 4Fe^{2+} + 8HCO_3^- + 2H_2O + 4\chi H_2PO_4^- \rightarrow 4Fe(OH)_3 + 4\chi Fe\text{-}P + 8CO_2 \quad (R9)$$

$$2O_2 + FeS \rightarrow SO_4^{=} + Fe^{2+} \quad (R10)$$

$$7O_2 + 2FeS_2 + 2H_2O \rightarrow 4SO_4^{=} + 2Fe^{2+} + 4H^+ \quad (R11)$$

$$2O_2 + H_2S + 2HCO_3^- \rightarrow SO_4^{=} + 2CO_2 + 2H_2O \quad (R12)$$

$$2O_2 + CH_4 \rightarrow CO_2 + 2H_2O \quad (R13)$$

$$MnO_2 + 2Fe^{2+} + 2\chi H_2PO_4^- + 2H_2O + 2HCO_3^- \rightarrow 2Fe(OH)_3 + 2\chi Fe\text{-}P + Mn^{2+} + 2CO_2 \quad (R14)$$

$$MnO_2 + H_2S + 2CO_2 \rightarrow Mn^{2+} + S_0 + 2HCO_3^- \quad (R15)$$

$$2Fe(OH)_3 + 2\chi Fe\text{-}P + H_2S + 4CO_2 \rightarrow 2Fe^{2+} + 2\chi H_2PO_4^- + S_0 + 4HCO_3^- + 2H_2O \quad (R16)$$

$$Fe^{2+} + H_2S \rightarrow FeS + 2H^+ \quad (R17)$$

$$SO_4^{=} + CH_4 + CO_2 \rightarrow 2HCO_3^- + H_2S \quad (R18)$$

$$4S_0 + 4H_2O \rightarrow 3H_2S + SO_4^{=} + 2H^+ \quad (R19)$$

$$FeS + H_2S \rightarrow FeS_2 + H_2 \quad (R20)$$

[a] Organic matter (OM) is of the form $(CH_2O)_a(NH_3)_b(H_3PO_4)_c$.
[b] χ denotes the ratio of adsorbed or coprecipitated phosphorus to iron oxyhydroxides.

with either a diffusive flux or a gradient of zero specified at the base of the model domain.

The model is solved numerically using the Method of Lines approach. Spatial derivatives in the PDEs are replaced by finite difference approximations, thus reducing the equations to ordinary differential equations (ODEs) that are then solved with an ODE integrator. The spatial domain therefore becomes a uniform one-dimensional lattice. A resolution of 1 mm is used for this study. Steep gradients, as seen in organic carbon profiles of sapropels, are problematic for standard finite difference schemes as they become smeared as time progresses (Boudreau, 1997, p. 346). To minimise this, a high-resolution central difference scheme was employed (Kurganov and Tadmor, 2000). The model definition and finite differencing scheme are coded in C and compiled into a library for use with the statistical programming package, R (R Development Core Team, 2006; Soetaert and Herman, 2009). An R script

passes the initial and boundary conditions, the model definition, and the user-specified parameters to the VODE ODE solver (Soetaert et al., 2010). VODE returns the model solution at requested times throughout the simulation.

Simulations presented here comprise of two phases: (1) an oxygen-depleted phase during which the sapropel is formed and (2) a burn-down phase where bottom waters have been reoxygenated. Prior to all simulations, the model is run to steady-state with present day parameters to eliminate the effects of initial conditions and to ensure that the state of the model at the outset is internally consistent and realistic.

3. MODEL APPLICATION

3.1. Dataset and parameters

A comprehensive sediment and pore water dataset is used pertaining to a deep basin, pelagic site in the eastern Mediterranean Sea: station SL114 located at 35°17.241′N, 21°24.519′E, 3.39 km water depth (Slomp et al., 2002). Profiles cover roughly the first half metre of sediment, thus encompassing the most recent sapropel (S1, 10.8–6.1 kyr cal. BP; de Lange et al., 2008). The model requires a number of site-specific environmental parameters: sedimentation rate, porosity, tortuosity, temperature, bioturbation depth and intensity, and sediment density. The mean sedimentation rate at the site is determined from the positions of the original sapropel boundaries, as evident from the solid phase barium profile (i.e., biogenic barite; Slomp et al., 2002), and the dates of the onset and termination of sapropel formation. The Ba profile exhibits the typical "broad peak with a quasi-Gaussian shape" and shows no signs of diagenetic mobilisation (Thomson et al., 1999; Slomp et al., 2002). The sedimentation rate is calculated as 3.3 cm kyr^{-1} and is assumed to be constant in time (Slomp et al., 2002). Solute diffusion coefficients for the model are taken from Van Cappellen and Wang (1995) and corrected for temperature as described by those authors. For these adjustments, a bottom water temperature of 13 °C is used (Slomp et al., 2002).

Porosity in the model is set at 0.7, which is the mean value at SL114 (Slomp et al., 2002), and is used to determine tortuosity (Boudreau, 1997, Eq. (4.120)). A constant porosity implies that compaction is absent. Although the hemipelagic sediment above and below the sapropel may undergo compaction, a higher porosity persists within the organic-rich layer (Slomp et al., 2002). To avoid the complexities of a spatially and temporally variable porosity profile, including regions that are resistant to compaction, we assumed a depth-averaged porosity. Despite this simplifying assumption, the model is able to reproduce observations well (see Section 4 and Fig. 1).

Bioturbation parameters for the model are taken from Basso et al. (2004) who estimated the mixed layer depth and biodiffusion coefficient at SL114 by means of the radioisotope tracer ^{210}Pb, determining values of 2 cm and 5 cm^2 kyr^{-1}, respectively. These values are comparable to other pelagic eastern Mediterranean sites (Basso et al., 2004), but are small compared to non-Mediterranean oceanic sites (cf. Boudreau, 1994). This is attributed to the scarcity of macrobenthos in the deep Mediterranean; it has been suggested that meiofauna are responsible for the majority of particle mixing that is observed (Basso et al., 2004). This meagre benthic community is likely the result of a low export of organic matter from oligotrophic surface waters. Due to the dearth of macrofauna, bioirrigation is omitted from the model. During sapropel formation anoxic bottom waters preclude the presence of benthic macrofauna and, consequently, the biodiffusion coefficient is set to zero at these times. Finally, sediment density is assumed to be 2.65 g cm^{-3}. These parameters are summarised in Table 3.

In addition to these site-specific parameters, general parameters relating to rate constants used by the model are required and are taken from the literature, with the exception of two parameters that are constrained by the model. Table 4 lists these parameters and their sources. Organic matter found in sapropel S1 is reasonably labile, degrading under oxic conditions with a rate constant, k_α, of 0.07 ± 0.02 yr^{-1} (Moodley et al., 2005). Accordingly, a value of 0.07 yr^{-1} was employed in the model. Nevertheless, anaerobic oxidation of organic matter operates at a much slower rate within sapropels. Moodley et al. (2005) performed oxic, anoxic, and sulphidic incubations with organic matter taken from sapropel S1 at four different sites in the Mediterranean. Results of this study demonstrate that the rate of sulphate reduction is substantially slower than aerobic respiration and is retarded further by the presence of sulphide. The model accounts for this by multiplying the remineralisation rate constant by an attenuation factor, Ψ, to retard degradation via sulphate reduction and methanogenesis. Ψ is constrained by the model (see Section 3.3).

3.2. Boundary conditions

3.2.1. Organic matter

Concentrations of organic carbon above and below the sapropel are effectively the same, with values of approximately 0.1%. Having resisted remineralisation under oxic conditions, this material is interpreted as being refractory. Likewise, the concentration of residual organic carbon within the oxidised portion of the sapropel is similar in magnitude suggesting that the depositional flux of refractory organic carbon has been relatively constant over time. Accordingly, the depositional flux of inert organic carbon is prescribed as an invariable 2.5 mmol m^{-2} yr^{-1}. The same rationale applies to refractory organic nitrogen and phosphorus, which are added at the sediment–water interface at constant fluxes of 0.96 mmol m^{-2} yr^{-1} and 0.112 mmol m^{-2} yr^{-1}, respectively.

The present day flux of reactive organic carbon to the sediment–water interface is calculated using the empirical model of Suess (1980):

$$J_G(z) = \frac{G_{pp}}{0.0238z + 0.212} \quad (3)$$

where G_{pp} is the primary production in the surface waters (gC m^{-2} yr^{-1}), z is water depth (m) and J_G is the depositional flux of organic carbon (g m^{-2} yr^{-1}). At site SL114, $z = 3.39$ km (Slomp et al., 2002) and $G_{pp} = 26$ gC m^{-2} yr^{-1}

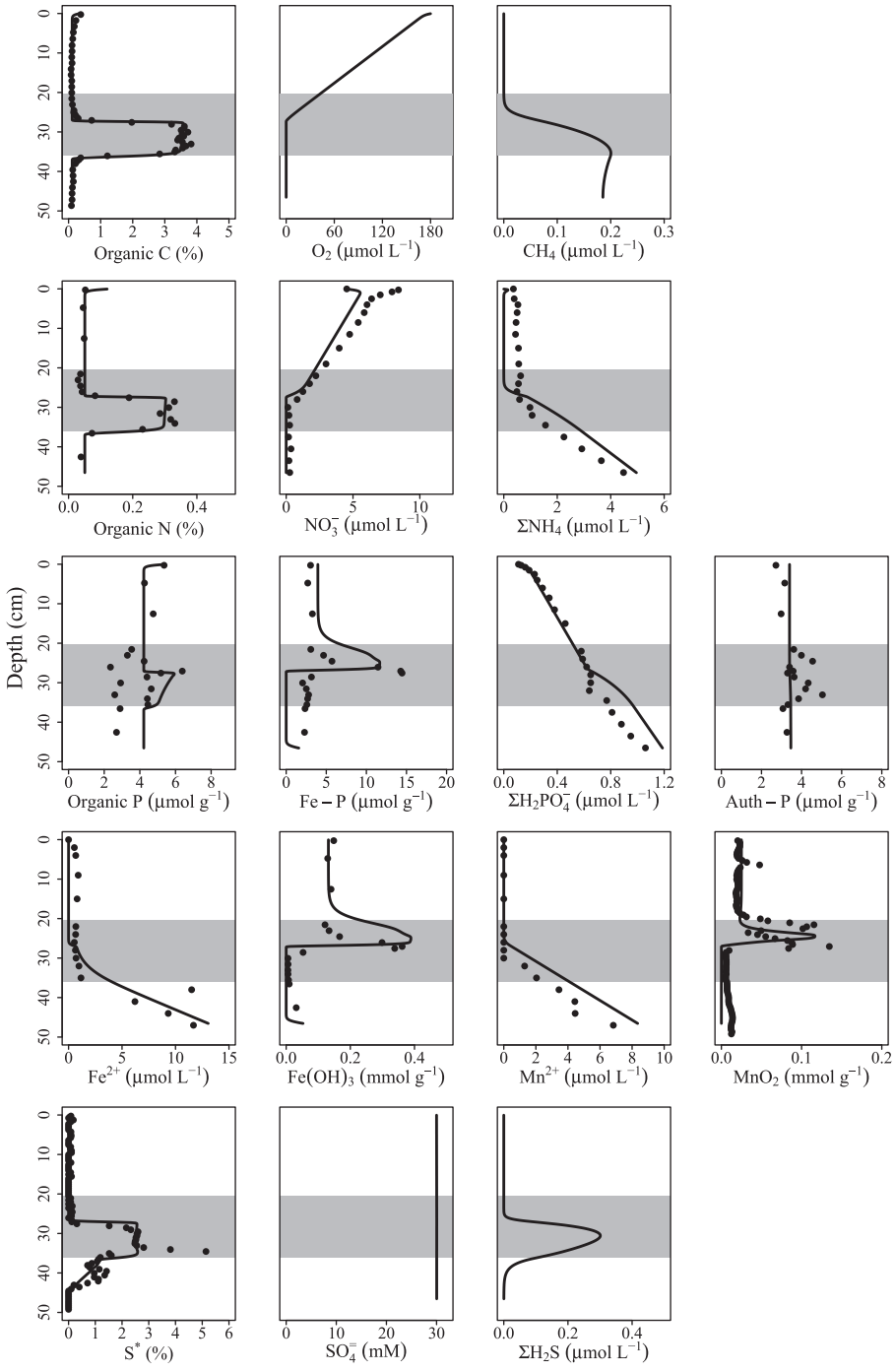

Fig. 1. A comparison between profiles generated by the diagenetic model (solid lines) and data from site SL114 (filled circles; Slomp et al., 2002). The shaded area represents the original extent of the sapropel. *The solid phase sulphur profile is the sum of S_0, FeS, and FeS_2, although pyrite accounts for >98% of the depth-integrated profile.

in the eastern Mediterranean (Dugdale and Wilkerson, 1988) furnishing a depositional flux of 27 mmol m^{-2} yr^{-1}. The depositional flux of reactive organic matter during sapropel formation is constrained by the model (Section 3.3). The total flux of organic nitrogen (i.e., reactive + refractory) to the sediment–water interface under present day conditions is determined from the total organic carbon flux using a C:N ratio of 106:30, which differs from the Redfield ratio value (106:16) in order to produce enough ammonia to support the nitrate peak observed near the sediment–water interface (Fig. 1). Nevertheless, because *ex situ* measurements of nitrate potentially exhibit steeper near-surface gradients than *in situ* measurements, nitrate may be somewhat overestimated in the vicinity of the sediment–water interface (Hall et al., 2007). The measured C:N ratio of organic matter within the sapropel is approximately

Table 3
Environmental and transport parameters used by the diagenetic model.

Parameter	Value	Units	Source
Porosity, ϕ	0.7	—	a
Solid volume fraction, $\phi_s = 1 - \phi$	0.3	—	a
Tortuosity, $\theta^2 = 1 - 2\ln\phi$	1.71	—	b
Sediment density	2.65	g cm^{-3}	—
Bottom water temperature	13	°C	a
Biodiffusion coefficient at surface, D_{b0}	5.0	cm^2 kyr^{-1}	c
Mixed layer depth, x_b	2.0	cm	c
Burial velocity, v	3.3	cm kyr^{-1}	d
P:Fe ratio for Fe-P, χ	0.03	—	a

[a]Slomp et al. (2002).
[b]Boudreau (1997).
[c]Basso et al. (2004).
[d]This study based on data from Slomp et al. (2002) and dating from de Lange et al. (2008).

Table 4
Reaction parameters for the diagenetic model. Limiting concentrations double as inhibition coefficients in the Monod scheme (Boudreau, 1996).

Parameter	Symbol	Value	Units	Source	Range given by source, ⟨Values used by source⟩
Decay constant for organic matter type α	k_α	0.07	yr^{-1}	a	0.07 ± 0.02
Decay constant for organic matter type β	k_β	0	yr^{-1}	—	—
Limiting concentration of O_2	k_{O_2}	0.001	mM	b	0.001–0.03, ⟨0.02⟩
Limiting concentration of NO_3^-	$k_{NO_3^-}$	0.004	mM	b	0.004–0.08, ⟨0.002⟩
Limiting concentration of MnO_2	k_{MnO_2}	16	μmol g^{-1}	b	4–32, ⟨4, 16, 32⟩
Limiting concentration of $Fe(OH)_3$	$k_{Fe(OH)_3}$	65	μmol g^{-1}	b	65–100, ⟨65, 100⟩
Limiting concentration of $SO_4^{=}$	$k_{SO_4^{=}}$	1.6	mM	b	1.6, ⟨1.6⟩
Attenuation factor for $SO_4^{=}$ reduction	Ψ	0.00157	—	c	—
Acceleration factor for P^{α}_{org} remineralisation	ε	30	—	c	—
Rate constant for (R7)	k_1	39,000	mM^{-1} yr^{-1}	d	39,000, ⟨39,000⟩
Rate constant for (R8)	k_2	20,000	mM^{-1} yr^{-1}	b	800–20,000, ⟨5000,10,000⟩
Rate constant for (R9)	k_3	140,000	mM^{-1} yr^{-1}	b	140,000, ⟨140,000⟩
Rate constant for (R10)	k_4	300	mM^{-1} yr^{-1}	b	300, ⟨300⟩
Rate constant for (R11)	k_5	1	mM^{-1} yr^{-1}	d	1, ⟨1⟩
Rate constant for (R12)	k_6	160	mM^{-1} yr^{-1}	b	⩾160, ⟨160⟩
Rate constant for (R13)	k_7	10,000	mM^{-1} yr^{-1}	b	10,000, ⟨10,000⟩
Rate constant for (R14)	k_8	2	mM^{-1} yr^{-1}	d	2, ⟨2⟩
Rate constant for (R15)	k_9	20	mM^{-1} yr^{-1}	b	⩽100,000, ⟨20⟩
Rate constant for (R16)	k_{10}	8	mM^{-1} yr^{-1}	b	⩽100, ⟨8⟩
Rate constant for (R17)	k_{11}	14,800	mM^{-1} yr^{-1}	d	14,800, ⟨14,800⟩
Rate constant for (R18)	k_{12}	0.01	mM^{-1} yr^{-1}	b	0.01, ⟨0.01⟩
Rate constant for (R19)	k_{13}	3	yr^{-1}	d	3, ⟨3⟩
Rate constant for (R20)	k_{14}	3.15	mM^{-1} yr^{-1}	e	3.15

[a]Moodley et al. (2005).
[b]Wang and Van Cappellen (1996).
[c]Constrained by the model.
[d]Berg et al. (2003).
[e]Rickard (1997).

106:7.6. Accordingly, this value is used in the model during the sapropel formation phase of simulations. Throughout all simulations the Redfield ratio is assumed for phosphorus in organic matter, i.e., the C:P ratio is set as 106:1. Due to enhanced remineralisation of organic phosphorus relative to organic carbon under oxygen-depleted conditions, the present day C:P ratio observed within sapropel S1 does not reflect the C:P ratio of organic matter deposited during sapropel formation.

3.2.2. Solutes

During sapropel formation the bottom water concentrations of all solutes — with the exception of H_2S and $SO_4^{=}$ — are assumed to be zero. (The rationale for a non-zero hydrogen sulphide concentration is discussed in Section 4.2.2.) Presently, bottom water oxygen concentrations in the eastern Mediterranean are approximately 170–200 μmol L^{-1} (Van Santvoort et al., 1996) and, therefore, a value of 180 μmol L^{-1} is used during the burn-down

phase. The presence of free oxygen precludes the presence of hydrogen sulphide, which is thus set to zero at the model's upper boundary when the bottom water is oxic. In accordance with the dataset, the concentration of nitrate at the sediment–water interface is set at the present day value of 4.53 μmol L^{-1} during the burn-down phase, while ammonium, dissolved manganese, and iron are all set to zero (Slomp et al., 2002). The diffusive fluxes at the base of the model domain for Fe^{2+}, Mn^{2+}, NH_4^+ and $H_2PO_4^-$ are determined from the dataset as −0.56, −0.24, −0.35, and −0.017 mmol m^{-2} yr^{-1}, respectively, and are assumed to be constant throughout the simulations. Note that these fluxes are negative because downwards is the positive direction in the model domain. All other solutes have a gradient of zero at the lower boundary of the model.

3.2.3. Solids

Under present conditions, no particulate sulphur compounds are deposited at site SL114 and, consequently, the depositional fluxes of elemental sulphur, iron monosulphide, and pyrite are set to zero when the bottom water is oxygenated. The iron sulphide flux, however, is non-zero during sapropel formation due to precipitation in sulphidic bottom waters and is constrained by fitting the model to observations. The depositional fluxes of iron and manganese oxides are set to zero during the deposition of S1. The present day fluxes of these species are estimated by model fitting. 'Authigenic' phosphorus (i.e., carbonate fluorapatite) is neither produced or consumed in the sediment (Slomp et al., 2002) and is thus deposited at the sediment surface at a constant rate, as indicated by its vertical profile (Fig. 1). The depositional flux of iron-bound phosphorus is determined by combining the depositional flux of iron oxyhydroxides with the average observed P:Fe ratio (0.03). Table 5 summarises all of the boundary conditions.

3.3. Constraining sulphate reduction and organic matter deposition

Organic matter degradation in Mediterranean Sea sediments is markedly slower under anoxic conditions (Moodley et al., 2005). To simulate this phenomenon, the rates of sulphate reduction and methanogenesis are a fraction, Ψ, of the remineralisation rate by more energetically favourable pathways. The value of this parameter is determined using the present day Fe^{2+} profile. Currently, the flux of dissolved iron from below the sapropel is consumed entirely at the lower boundary of the organic-rich layer through reaction with hydrogen sulphide to form iron monosulphide (Reaction (R17); Fig. 1). Since H_2S is predominantly produced by sulphate reduction and the flux of iron from below the sapropel is known from the dataset, Ψ can be determined by fitting the model generated Fe^{2+} profile to the measured profile. Adopting this approach, Ψ is estimated as $\sim 1.57 \times 10^{-3}$. The resulting sulphate reduction rate constant (1.1×10^{-5} yr^{-1}) is 2 orders of magnitude greater than predicted by Tromp et al.'s (1995) empirical relationship, but is not unreasonable considering that the sulphate reduction rate constant has a range of at least 7 orders of magnitude (Tromp et al., 1995).

The present day organic carbon content in the unoxidised region of the sapropel represents the difference between the amount of organic matter initially deposited and the amount that has been remineralised anaerobically. Thus, as the rate of sulphate reduction and current concentration of organic carbon in the unoxidised portion of the sapropel are known, the depositional flux of organic carbon during sapropel formation can be calculated.

4. RESULTS AND DISCUSSION

After running the model to steady-state with present day conditions, the simulation began at the onset of anoxia, 10.8 kyr cal. BP, with appropriate boundary conditions (Table 5). At 6.1 kyr cal. BP, these boundary conditions are replaced to reflect the reoxygenation of bottom waters and the model continues until present day. Sediment and pore water profiles are then output by the model and compared with the dataset (Fig. 1). Simulated profiles show that the model provides an excellent description of sapropel formation and post-depositional alteration.

4.1. Organic-rich layers

4.1.1. Remineralisation

Microbially mediated organic matter decomposition plays an important role in driving the biogeochemistry of marine sediments. Sapropels are rich in organic matter, by definition, and therefore exert significant influence on the biogeochemical function of sediments. As a result of transient redox conditions associated with sapropel formation, remineralisation pathways vary with time. During sapropel deposition, organic matter degradation is dominated by sulphate reduction due to an absence of oxidants with higher energy yields and an abundance of sulphate (Fig. 2). Because sulphate reduction progresses significantly slower than aerobic respiration (Moodley et al., 2005), the rate of remineralisation during sapropel formation is markedly lower than after the reoxygenation of the bottom waters. The depth-integrated sulphate reduction rate gradually increases during sapropel deposition, as organic matter accumulates in the sediment.

Following the reintroduction of oxygen to the overlying waters, organic matter decomposition exhibits a sharp peak due to a steep oxygen gradient at the sediment–water interface and, thus, a large diffusive flux of oxygen into the sediment. As the organic-rich layer is oxidised and sediment accumulates at the surface, the redox boundary migrates away from the sediment–water interface (inset plot, Fig. 2) decreasing the gradient of the oxygen profile and, consequently, the influx of oxygen. That is to say, the flux of oxygen across the sediment–water interface is inversely proportional to the depth of the redox boundary. The location of the redox boundary is the sum of the burn-down depth (BDD) and the amount of sediment accumulated during the oxic phase. BDD is defined as the amount of

Table 5
Boundary conditions for the diagenetic model.

Component	Boundary conditions: anoxic phase		Boundary conditions: oxic phase	
	$x = 0$	$x = x_{max}$	$x = 0$	$x = x_{max}$
C^{α}_{org}	$J_{C^{\alpha}_{org}} = 84.0$	$\frac{\partial[C^{\alpha}_{org}]}{\partial x} = 0$	$J_{C^{\alpha}_{org}} = 26.8$	$\frac{\partial[C^{\alpha}_{org}]}{\partial x} = 0$
C^{β}_{org}	$J_{C^{\beta}_{org}} = 2.5$	$\frac{\partial[C^{\beta}_{org}]}{\partial x} = 0$	$J_{C^{\beta}_{org}} = 2.5$	$\frac{\partial[C^{\beta}_{org}]}{\partial x} = 0$
N^{α}_{org}	$J_{N^{\alpha}_{org}} = 5.24$	$\frac{\partial[N^{\alpha}_{org}]}{\partial x} = 0$	$J_{N^{\alpha}_{org}} = 7.32$	$\frac{\partial[N^{\alpha}_{org}]}{\partial x} = 0$
N^{β}_{org}	$J_{N^{\beta}_{org}} = 0.96$	$\frac{\partial[N^{\beta}_{org}]}{\partial x} = 0$	$J_{N^{\beta}_{org}} = 0.96$	$\frac{\partial[N^{\beta}_{org}]}{\partial x} = 0$
P^{α}_{org}	$J_{P^{\alpha}_{org}} = 0.690$	$\frac{\partial[P^{\alpha}_{org}]}{\partial x} = 0$	$J_{P^{\alpha}_{org}} = 0.164$	$\frac{\partial[P^{\alpha}_{org}]}{\partial x} = 0$
P^{β}_{org}	$J_{P^{\beta}_{org}} = 0.112$	$\frac{\partial[P^{\beta}_{org}]}{\partial x} = 0$	$J_{P^{\beta}_{org}} = 0.112$	$\frac{\partial[P^{\beta}_{org}]}{\partial x} = 0$
O_2	$[O_2] = 0$	$\frac{\partial[O_2]}{\partial x} = 0$	$[O_2] = 0.18$	$\frac{\partial[O_2]}{\partial x} = 0$
NO_3^-	$[NO_3^-] = 0$	$\frac{\partial[NO_3^-]}{\partial x} = 0$	$[NO_3^-] = 0.00453$	$\frac{\partial[NO_3^-]}{\partial x} = 0$
MnO_2	$J_{MnO_2} = 0$	$\frac{\partial[MnO_2]}{\partial x} = 0$	$J_{MnO_2} = 0.7$	$\frac{\partial[MnO_2]}{\partial x} = 0$
$Fe(OH)_3$	$J_{Fe(OH)_3} = 0$	$\frac{\partial[Fe(OH)_3]}{\partial x} = 0$	$J_{Fe(OH)_3} = 3.5$	$\frac{\partial[Fe(OH)_3]}{\partial x} = 0$
$SO_4^{=}$	$[SO_4^{=}] = 30$	$\frac{\partial[SO_4^{=}]}{\partial x} = 0$	$[SO_4^{=}] = 30$	$\frac{\partial[SO_4^{=}]}{\partial x} = 0$
Mn^{2+}	$[Mn^{2+}] = 0$	$J_{Mn^{2+}} = -0.244$	$[Mn^{2+}] = 0$	$J_{Mn^{2+}} = -0.244$
Fe^{2+}	$[Fe^{2+}] = 0$	$J_{Fe^{2+}} = -0.561$	$[Fe^{2+}] = 0$	$J_{Fe^{2+}} = -0.561$
ΣNH_4^+	$[\Sigma NH_4^+] = 0$	$J_{\Sigma NH_4^+} = -0.353$	$[\Sigma NH_4^+] = 0$	$J_{\Sigma NH_4^+} = -0.353$
$\Sigma H_2PO_4^-$	$[\Sigma H_2PO_4^-] = 0$	$J_{\Sigma H_2PO_4^-} = -0.017$	$[\Sigma H_2PO_4^-] = 0$	$J_{\Sigma H_2PO_4^-} = -0.017$
ΣH_2S	$[\Sigma H_2S] = 0.0125$	$\frac{\partial[\Sigma H_2S]}{\partial x} = 0$	$[\Sigma H_2S] = 0$	$\frac{\partial[\Sigma H_2S]}{\partial x} = 0$
CH_4	$[CH_4] = 0$	$\frac{\partial[CH_4]}{\partial x} = 0$	$[CH_4] = 0$	$\frac{\partial[CH_4]}{\partial x} = 0$
S_0	$J_{S_0} = 0$	$\frac{\partial[S_0]}{\partial x} = 0$	$J_{S_0} = 0$	$\frac{\partial[S_0]}{\partial x} = 0$
FeS	$J_{FeS} = 0$	$\frac{\partial[FeS]}{\partial x} = 0$	$J_{FeS} = 0$	$\frac{\partial[FeS]}{\partial x} = 0$
FeS_2	$J_{FeS_2} = 10$	$\frac{\partial[FeS_2]}{\partial x} = 0$	$J_{FeS_2} = 0$	$\frac{\partial[FeS_2]}{\partial x} = 0$
Fe-P	$J_{Fe\text{-}P} = 0$	$\frac{\partial[Fe\text{-}P]}{\partial x} = 0$	$J_{Fe\text{-}P} = 0.105$	$\frac{\partial[Fe\text{-}P]}{\partial x} = 0$
Auth-P	$J_{Auth\text{-}P} = 0.0902$	$\frac{\partial[Auth\text{-}P]}{\partial x} = 0$	$J_{Auth\text{-}P} = 0.0902$	$\frac{\partial[Auth\text{-}P]}{\partial x} = 0$

Fluxes have units of mmol m^{-2} yr^{-1}; concentrations have units of mmol L^{-1}; spatial derivatives have units of μmol cm^{-4}.

the organic-rich layer that has been oxidised in units of length (Appendix C). The migration of the redox boundary is quasi-linear in time and, consequently, the organic matter remineralisation rate plateaus after several thousand years as the system approaches a steady-state (Fig. 2). Note, however, that the asymptote for depth-integrated remineralisation rate is not zero since this metric includes the entire model domain and thus the oxidation of organic matter deposited during the oxic period. Relative to aerobic respiration, denitrification and sulphate reduction play minor roles in organic matter degradation, while all other pathways are negligible throughout the simulation. Iron oxyhydroxides and manganese oxides form at the redox boundary and interact little with the organic-rich layer due a relatively low rate and depth of biogenic mixing. Methanogenesis is virtually absent since sulphate is abundant throughout the model domain.

Integrating the remineralisation rate with respect to time furnishes the total amount of organic carbon oxidised over the considered interval. Since remineralisation is oxygen limited and the flux of oxygen into the sediment is an inverse function of time, burn-down depth is therefore logarithmic in form (inset plot, Fig. 2). The extent of burn-down, however, is controlled by environmental parameters whose impact have been the subject of debate (e.g., Jung et al., 1997). The model presented above provides a tool with which to explore and quantify the effect that these parameters have on sapropel oxidation.

4.1.2. Controls on burn-down

To examine the sensitivity of sapropel burn-down to environmental conditions, the simulation described above was rerun with pertinent parameters varied by ±25%, while all other parameters were kept fixed. The resulting changes in present day burn-down depth (BDD) were recorded and compiled into Fig. 3. In this figure, two bars are plotted for each parameter: a white bar represents the percentage change in burn-down depth due to a 25% increase in the parameter, while a black bar corresponds to a 25% decrease. The parameters considered were those thought to change most between different settings: porosity, sedimentation rate, depth and intensity of bioturbation, depositional flux of organic carbon during sapropel formation, depositional flux of organic carbon after sapropel

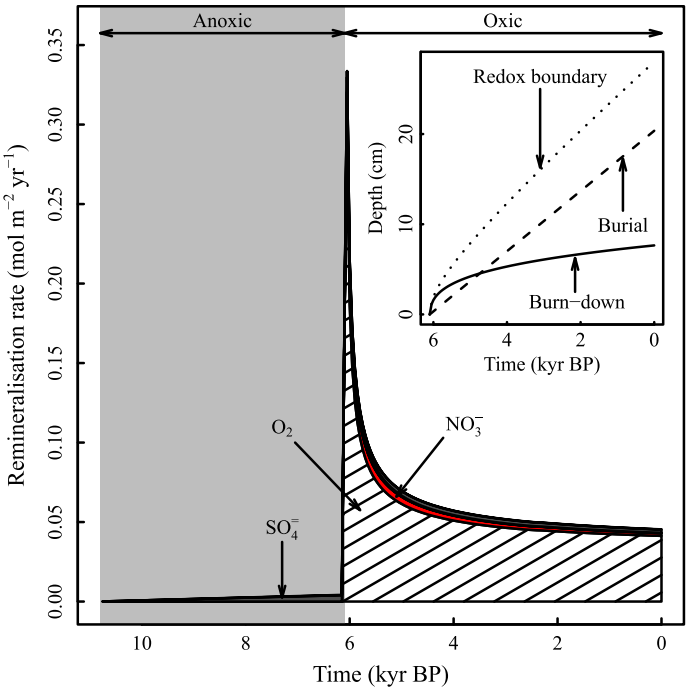

Fig. 2. Depth-integrated organic matter degradation rate for remineralisation pathways during the formation and post-depositional alteration of sapropel S1: aerobic respiration (O_2); denitrification (NO_3^-); and sulphate reduction ($SO_4^=$). All other pathways are omitted as they are negligible in magnitude. Inset is a plot showing the depth of the redox boundary during the simulation. The contributions of burn-down and burial (i.e., sedimentation) to the depth of redox boundary are also plotted. Note that the diffusive flux of oxygen to the organic-rich layer is inversely proportional to the depth of the redox boundary.

formation, organic matter degradation rate, sulphate reduction rate, bottom water oxygen concentration during the oxidation phase, and depositional flux of pyrite. Of these parameters, most only caused the burn-down curve to deviate slightly from the original simulation, whilst five parameters exhibited a marked influence: porosity, bottom water oxygen concentration, depositional flux of organic carbon during sapropel formation, sedimentation rate, and pyrite depositional flux (Fig. 3).

At site SL114, the depth and intensity of bioturbation are relatively small at 2 cm and 5 cm^2 kyr^{-1}, respectively (Basso et al., 2004), and consequently have only a very minor impact on sapropel oxidation. The rate of aerobic organic matter decomposition also has a negligible influence on sapropel oxidation, because, as seen in the preceding section, organic matter remineralisation is for the most part limited by oxygen availability. As a result, varying the rate constant by ±25% produces a less than 2% change in BDD. Owing to oligotrophic surface waters, the present-day flux of organic carbon to eastern Mediterranean sediments is quite modest consuming only a small amount of oxygen during remineralisation. Therefore, varying this flux is inconsequential and, like the remineralisation rate constant, evokes a less than 2% response in BDD. Sulphate reduction progresses at a relatively slow rate — 3 orders of magnitude slower than aerobic oxidation — and, thus, plays only a very minor role in the decomposition of organic matter for S1.

Fluxes of pyrite and organic matter during sapropel formation affect post-sapropel burn-down as these compounds regulate the oxygen demand of the sapropel. Higher depositional fluxes yield a higher concentration within the sapropel, requiring a greater amount of oxidant per centimetre of BDD, thus slowing down the rate of burn-down. Sedimentation rate influences sapropel oxidation in two opposing ways. First, post-sapropel sedimentation rate affects the position of the redox front (inset plot, Fig. 2) and therefore gradient of the oxygen profile, which regulates the diffusive flux into the sediment. Increasing the sedimentation rate causes the redox front to move away from the sediment–water interface more rapidly, meaning that the influx of oxygen declines more rapidly, as a result. In contrast, increasing the sedimentation rate during sapropel deposition while maintaining the same depositional flux of organic material leads to a lower concentration of organic matter in the sapropel and to a thicker organic-rich layer. Thus, during post-sapropel remineralisation less oxidant is required per centimetre of sapropel, hence an increased burn-down depth. Of the two influences, the latter dominates in the considered case. When using these results to interpret field data, it should be kept in mind that various environmental conditions may change in concert. For example, field data for the Aegean and Adriatic show that almost no burn-down of the sapropel occurs at sites with markedly (i.e., order of magnitude) higher sedimentation rates (e.g., sites SL60 and MD90-917; Slomp et al., 2004). This is likely because these sites are located at shallower water depths and also receive an increased flux of organic matter when compared to deep sea low sedimentation rate sites. Bottom water oxygen concentration plays an important role in

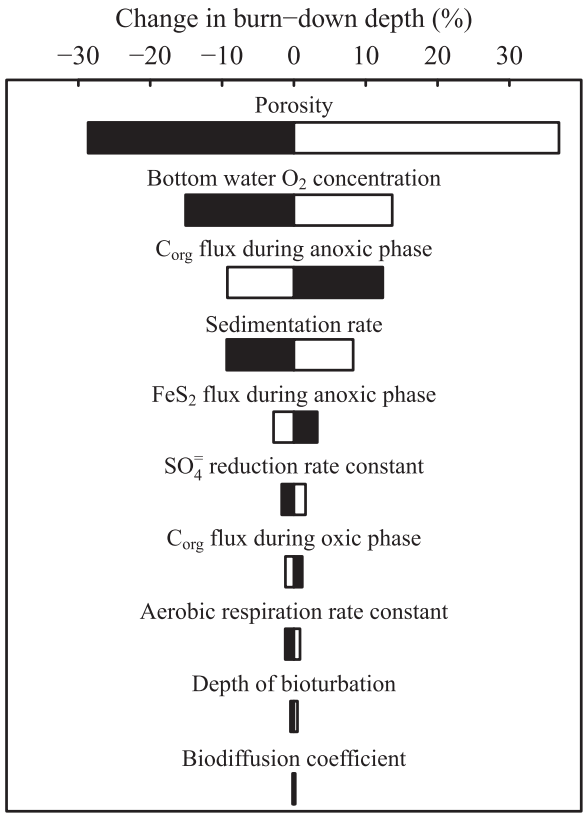

Fig. 3. A plot showing the sensitivity of the present day burn-down depth to various environmental parameters. The white and black bars relate to a 25% increase and decrease in the parameters, respectively.

burn-down since it affects the flux of oxygen into the sediment and aerobic respiration is the chief remineralisation pathway (Fig. 2). Indeed, oxygen flux is a linear function of bottom water oxygen concentration, which therefore exerts a notable influence over the depth of burn-down. Finally, porosity exhibits the most influence on the oxidation of the organic-rich layer since changes in porosity simultaneously affect the flux of oxygen to the organic-rich layer and the amount of organic material and pyrite per centimetre of sapropel. These factors compound one another resulting in a marked response in burn-down depth. Nevertheless, the range of variation (0.525–0.875) is larger than is typically observed in deep sea sediments and, therefore, porosity variation is likely to have less impact in nature. Broadly speaking, the sensitivity analysis demonstrates that the most influential parameters with regard to burn-down depth are those that exert the greatest impact on the oxygen demand of the sapropel and the flux of oxygen from the water column.

4.1.3. Conditions for formation

In addition to establishing the factors that regulate the oxidation of organic-rich layers, the model is also used to identify the conditions under which these geological features are formed. In general, sapropels are the product of enhanced organic matter deposition, oxygen-depleted bottom waters, or a combination of these two factors. The results of the simulation described above show that the flux of reactive organic carbon to the sediment–water interface during S1 formation at station SL114 was approximately three times the present day flux and bottom waters were not only anoxic but sulphidic: a depositional flux of FeS or pyrite is needed to reproduce solid phase sulphur and iron oxyhydroxide profiles (Table 5). The behaviour of these species are tightly linked since iron oxyhydroxides found at the redox front are mostly formed by the oxidation of pyrite within the organic layer, as discussed in detail below. The absence of these iron oxyhydroxides impacts on iron-bound phosphorus and, consequently, on pore water phosphate profiles. With these exceptions, all pore water and sediment profiles can be reproduced assuming an anoxic but non-sulphidic water column. Indeed, even when bottom waters are oxic during the formation phase these profiles can be reproduced providing the depositional flux of organic matter is sufficiently large. Fig. 4 shows the reactive organic carbon flux needed to produce a sapropel comparable to S1 at a range of bottom water oxygen concentrations during the formation phase. Present day conditions are also plotted illustrating that both a decline in bottom water oxygen conditions and an enhanced input of organic matter are needed for a sapropel-like feature to form today. A clear linear relationship exists demonstrating that the required increase in the organic carbon depositional flux is directly proportional to the increase in bottom water oxygen. These results show that both the organic carbon content of a sapropel and an estimate of bottom water redox conditions are needed in order to constrain the depositional flux (Calvert and Pedersen, 1993). Use of palaeoredox indicators, such as C_{org}:P_{org} ratios (Kraal et al., 2010a), C_{org}:S ratios (Leventhal, 1995), and trace metals (Brumsack, 2006), would aid the unambiguous reconstruction of the setting under which the organic-rich layer was formed.

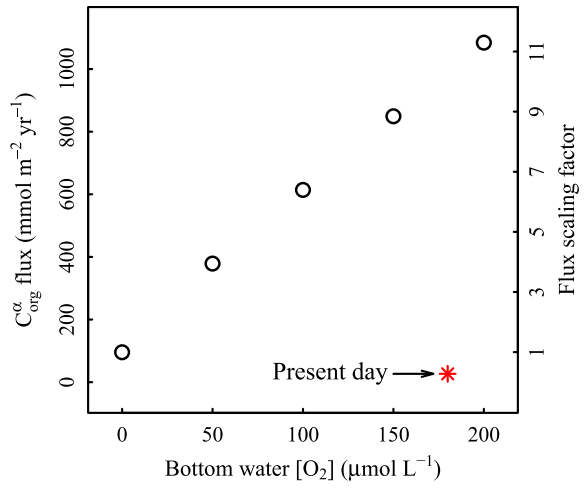

Fig. 4. The depositional flux of reactive organic carbon required to form an organic-rich layer like S1 at SL114 under various bottom water oxygen concentrations. The left-hand axis gives the organic carbon depositional flux (mmol m^{-2} yr^{-1}); the right-hand axis gives the flux as a multiple of the flux under anoxic bottom waters. The asterisk represents present day conditions.

The organic carbon content of an organic-rich layer (when non-zero) is a linear function of the depositional flux under constant redox conditions, although the gradient of this function depends on the oxygen concentration of the overlying waters (Fig. 5). Therefore, the organic carbon content of an organic-rich layer is directly proportional to the depositional flux under fully anoxic conditions and may be used as a proxy of organic matter input under such circumstances. The gradient decreases with increasing bottom water oxygen concentration meaning that an elevated flux of organic matter to the sediment has less impact at higher oxygen concentrations due to higher remineralisation rates. Consequently, organic-rich layers with high C_{org} contents (for example, greater than 15%, such as some black shales (e.g., Kraal et al., 2010b) and Pliocene sapropels (e.g., Slomp et al., 2004)) imply that both overlying waters were oxygen depleted and primary production elevated, otherwise the increase in primary productivity that must be produced and maintained under oxic conditions appears to be prohibitively high (Fig. 5).

4.2. Sediment biogeochemistry

4.2.1. Manganese enrichments

The model generated manganese oxide profile exhibits a peak immediately above the oxidation front, which is also evident in the dataset (Fig. 1). This peak is actively forming in the model, as in nature, due to dissolved manganese diffusing upwards from below the sapropel and reacting with oxygen that is diffusing downwards from the sediment–water interface (Van Santvoort et al., 1996). The magnitude of the generated peak is slightly lower than observed, suggesting that the manganese flux from below was somewhat higher in the past. A second peak is evident in the field data at the original upper boundary of the sapropel, which is not reproduced by the model. Indeed, the inability of the model to produce the upper peak supports the hypothesis that it is not of diagenetic origin (cf. Pruysers et al., 1993), but is a depositional feature (Van Santvoort et al., 1996; Reitz et al., 2006), likely due to the precipitation of manganese oxides in the water column following reventilation of deep waters (Mangini et al., 1991). Fig. 3 of Thomson et al. (1999) summarises this scenario. Above the manganese enrichment, the concentration of MnO_2 in the sediment is relatively constant, which suggests an invariable depositional flux relative to the mineral matrix under oxic bottom waters. Nevertheless, there is a small peak in the profile at 6.4 cm depth, which corresponds to an ash layer. While the location of the peak suggests that it is too young to have been produced by the Santorini eruption, the feature is most certainly depositional and, therefore, should not be reproduced by the model (Slomp et al., 2002).

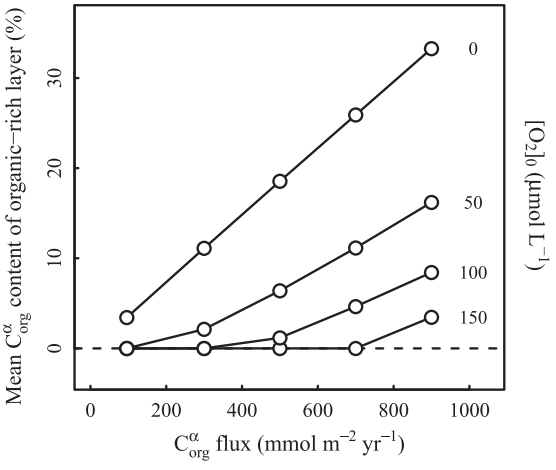

Fig. 5. The relationship between the depositional flux of reactive organic carbon and the mean reactive organic carbon content of the unoxidised organic-rich layer under various redox conditions.

4.2.2. Iron and sulphur dynamics

Iron and sulphur cycling are inextricably linked during the deposition and subsequent oxidation of sapropel S1. The conceptual model outlining the behaviour and interaction of these elements has been largely developed by Passier et al. (1996, 1999) and is briefly outlined below.

Two end-member scenarios have been defined to describe iron and sulphur dynamics at times of sapropel formation. In the first case, low sulphide production within the organic-rich layer relative to the Fe^{2+} flux from below leads to pyrite formation within but not below the sapropel. Iron sulphides are also formed in the organic-rich layer through the reduction of detrital iron oxyhydroxides. In the alternative scenario, the rate of sulphate reduction is sufficiently high to lead to sulphidic bottom waters and the precipitation of iron sulphides in the water column that are subsequently deposited at the sediment–water interface. The downward flux of hydrogen sulphide from the water column and organic-rich layer exceeds the flux of dissolved iron from depth causing pyrite precipitation to occur beneath the organic-rich layer. The upshot is pyrite throughout the sapropel, due to deposition, and also beneath the sapropel, due to *in situ* formation.

Our results provide support for the latter regime during the formation of S1 at site SL114, as both sulphidic bottom waters and a depositional flux of either FeS or FeS_2 is needed to replicate the observed solid phase sulphur (i.e., pyrite) profile (Fig. 1). Specifically, the downward flux of hydrogen sulphide is insufficient to form pyrite below the organic-rich layer — as observed — unless bottom waters are sulphidic. The depth that the pyritic region extends below the organic-rich layer can be used to constrain the concentration of H_2S at the sediment–water interface, which is estimated as approximately 12.5 μmol L^{-1} during sapropel formation. In addition, a depositional flux of 10 mmol m^{-2} yr^{-1} for either FeS or FeS_2 is required to replicate the profile within the sapropel.

Simulations demonstrated that the form of the iron sulphide flux from the water column has little bearing on model results. If a depositional flux of FeS is prescribed, FeS_2 is quickly formed at the sediment–water interface through the reaction of iron monosulphide with hydrogen sulphide diffusing into the sediment from the water column. Alternatively, pyrite may be precipitated within the water column and then deposited on the seafloor. Because iron is the limiting factor in pyrite formation in this setting, the required

depositional flux is the same regardless of the form of iron sulphide that is deposited. In both cases, pyrite accounts for >98% of the solid phase sulphur plotted in Fig. 1.

Passier et al. (1999) observed that the microtexture of the pyrite found within and below sapropel S1 (site UM26) differs, suggesting different formation kinetics. Framboidal pyrite, found within the organic-rich layer, is indicative of rapid kinetics, whereas euhedral pyrite below the sapropel is formed more slowly. These observations bolster our findings that FeS_2 located within the sapropel is precipitated either in the water column or shortly after deposition at the sediment–water interface, while pyrite beneath the organic-rich layer is formed more slowly *in situ*. Additional support for sulphidic bottom waters and iron sulphide precipitation in the water column is provided by the quantities of organic carbon and solid phase sulphur present within the unoxidised portion of the sapropel (approximately 3.5% and 2.5%, respectively), which are characteristic of a euxinic regime (Leventhal, 1995).

The iron oxyhydroxide content in the hemipelagic sediment overlying the sapropel varies little with depth, suggesting a fairly constant deposition flux. Current depositional fluxes of iron oxides are, like manganese oxides, determined by fitting the model generated profile to field data. During sapropel formation, the flux is zero due to euxinic overlying waters. The peak in iron oxyhydroxides present at the upper edge of the organic-rich layer (i.e., the redox boundary) is actively forming, as is clearly illustrated by the presence of fresh magnetic minerals (Passier et al., 2001). The greater part of this peak is due to the aerobic oxidation of pyrite derived Fe^{2+}. Any dissolved iron that escapes oxidation and diffuses downwards from the redox boundary reacts with hydrogen sulphide produced by sulphate reduction within the unoxidised sapropel to form iron sulphide. Within the model, Fe^{2+} diffusing up from beneath the sapropel is largely consumed during iron sulphide production at the base of the organic-rich layer and not by iron oxyhydroxide formation, as has been previously suggested (i.e., Van Santvoort et al., 1996; Thomson et al., 1999).

4.2.3. Nitrogen cycling

Sedimentary nitrogen cycling (i.e., transformations of nitrogen species) under oxic bottom waters is typically dominated by remineralisation of organic nitrogen through aerobic respiration coupled to aerobic oxidation of the resulting ammonium to nitrate (Burdige, 2006). Removal of fixed nitrogen may take place through burial of organic nitrogen and, more importantly, denitrification. Fig. 6 details nitrogen cycling throughout the simulation described above.

Deposition of organic nitrogen — unlike organic carbon — is lower during sapropel formation owing to a higher C:N ratio exhibited during the anoxic phase, likely due to a shift in the composition of the autotroph community (Fig. 6a; Moodley et al., 2005). The rain of refractory organic nitrogen to the sediment–water interface is constant throughout the simulation as the residual organic nitrogen after oxidation is the same both within, above, and below the sapropel. As the organic-rich layer is deposited, the organic nitrogen content of the sediment increases linearly with time (Fig. 6b). The accumulation rate of organic nitrogen in the sediment is slightly less than the depositional flux

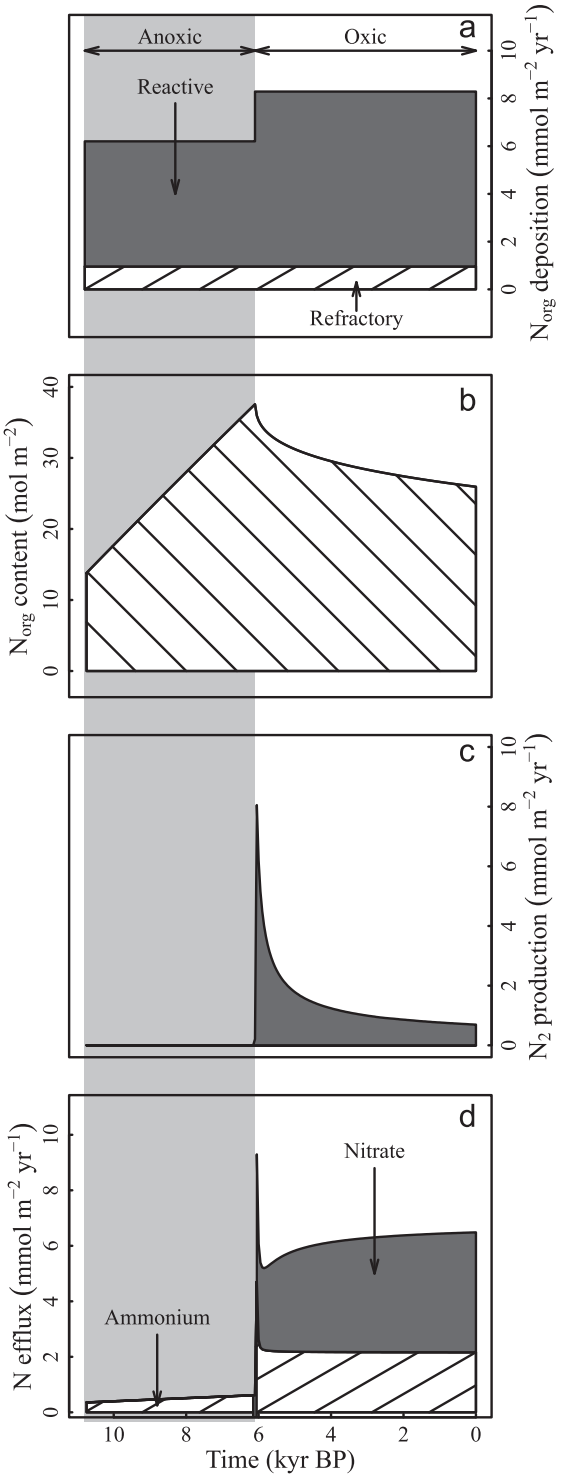

Fig. 6. Sedimentary nitrogen dynamics during the formation and post-depositional alteration of sapropel S1. Panel (a) shows the depositional fluxes of organic nitrogen during the simulation, while panel (b) plots the depth-integrated organic nitrogen content of the sediment column. Nitrogen is lost from sediments due to N_2 production (c) and the efflux of nitrate and ammonium (d).

due to anaerobic remineralisation of organic matter. When bottom waters become oxic the organic-rich layer is gradually oxidised, attenuating the amount of organic nitrogen retained in the sediment. Initially, the rate at which organic nitrogen is regenerated (i.e., the gradient of the line in Fig. 6b) is high, but decreases as organic matter remineralisation declines (Fig. 2). Immediately following the reventilation of deep waters, there is a marked spike in dinitrogen production corresponding to a peak in denitrification that declines quickly with time (Fig. 6c).

There is no release of nitrate to the water column from the sediments during the period of anoxia due to the absence of nitrification. Ammonium efflux gradually increases under anoxic bottom waters as the prescribed flux at the base of the model is augmented with ammonium produced by sulphate reduction and methanogenesis. Following reoxygenation of overlying waters, there is a spike in the nitrate efflux (Fig. 6d) due to the aerobic oxidation of the ammonium pulse released during organic matter remineralisation (Fig. 2). The flux of nitrate initially decreases as the rate of organic matter decomposition declines before increasing due to the redox boundary gradually moving downwards through burial and burn-down, since nitrate is consumed through denitrification at this boundary (inset in Fig. 2). After the pulse of ammonium associated with reoxygenation of the deep waters, the efflux of ammonium plateaus quickly and occurs solely due to the remineralisation of organic matter that is being deposited at that time. Likewise, the nitrate efflux approaches an asymptote as nitrate consumption by the organic-rich layer approaches zero (Fig. 6d). Finally, for the same reasons, N_2 production by denitrification approaches a constant value with increasing time (Fig. 6b).

Presently, nitrogen sources and sinks in the Mediterranean Sea are in balance, with burial in sediments accounting for 15% of nitrogen lost, while sedimentary denitrification represents 5.6% (Krom et al., 2004). Shifts in sedimentary nitrogen dynamics associated with sapropel formation, described above, represent a major perturbation to the nitrogen cycling on a basin-scale. For example, the organic nitrogen content of the upper half metre of sediment doubled during the deposition of S1 and denitrification was absent — yet immediately afterwards denitrification was 12 times higher than present day. These results demonstrate that the formation and oxidation of Mediterranean sapropels occur under a markedly different nitrogen cycling regime.

4.2.4. Phosphorus cycling

Quantifying phosphorus dynamics in the eastern Mediterranean is particularly pertinent as phosphorus is presently the limiting nutrient in the region (Krom et al., 1991). The mode of phosphorus cycling shifts in response to redox transitions, because phosphorus binds to iron oxyhydroxides, which are redox-sensitive (Slomp et al., 1996), and organic phosphorus remineralisation is enhanced relative to organic carbon under oxygen-depleted bottom waters (Ingall et al., 1993; Ingall and Jahnke, 1994; Slomp et al., 2002). The simulation described above allows the influence of transient redox conditions on phosphorus fluxes, retention, and speciation to be explored quantitatively, as shown in Fig. 7.

The depositional fluxes of phosphorus species are shown in Fig. 7a. For reasons discussed previously, refractory organic phosphorus has a constant rate of deposition. Reactive organic phosphorus supply to the sediment is higher during the anoxic phase due to an increased rain of organic matter associated with elevated primary productivity. Conversely, the depositional flux of phosphorus-bearing iron oxyhydroxides is zero under anoxic conditions reflecting reductive dissolution in the water column, and then increases following reoxygenation of deep waters. Organic phosphorus builds up in sediments during the period of anoxia as a result of an elevated flux of organic matter to the sediment in concert with enhanced preservation due to the absence of oxygen. Accumulation of organic phosphorus is not proportional to the organic carbon content, however, because of faster regeneration of organic phosphorus relative to organic carbon (see Section 2.2). Model fitting suggests that organic phosphorus is remineralised around 30 times faster than organic carbon in the considered scenario. Consequently, burial of the organic-rich layer constitutes only a small long-term phosphorus sink, in contrast with nitrogen.

Authigenic phosphorus is deposited at the sediment–water interface at a constant rate throughout the simulation and is not require to be produced or consumed within the sediment to balance the phosphorus budget (Slomp et al., 2002), meaning that the depth-integrated authigenic phosphorus content of the sediment is temporally invariable. Indeed, if authigenic phosphorus formation is included in the model using the kinetics and parameters of Slomp et al. (1996) there is a negligible amount precipitated due to low phosphate concentrations, which reach a maximum of 6.5 $\mu mol\ L^{-1}$. The iron-bound phosphorus content of the sediment declines when bottom waters become euxinic due to hydrogen sulphide diffusing into the underlying sediment from the water column, reducing iron oxyhydroxides and liberating associated phosphorus. As a result, there is an initial peak in phosphate efflux at the onset of euxinia (Fig. 7c), although if bottom waters are anoxic but not sulphidic the peak is absent (results not shown). Dissolution of iron oxyhydroxides and enhanced remineralisation of organic phosphorus mean that the benthic efflux of phosphate during S1 formation is elevated relative to present day conditions (Slomp et al., 2002). The release of phosphate under anoxic conditions is around 3.5 times higher than the current efflux immediately before reventilation of deep waters. When bottom waters become oxic again there is a peak in organic matter remineralisation (Fig. 2), which generates a corresponding pulse in benthic phosphate release (Fig. 7c).

Enhanced organic phosphorus remineralisation and dissolution of phosphorus-bearing iron oxyhydroxides during euxinia means that despite phosphorus deposition doubling for a period of 4.7 kyr, the total solid phase phosphorus content of the sediment is lower at the end of the simulation than at the outset. This is due to an elevated efflux of phosphate under euxinic conditions, as well as a substantial phosphate pulse from the sediments immediately following

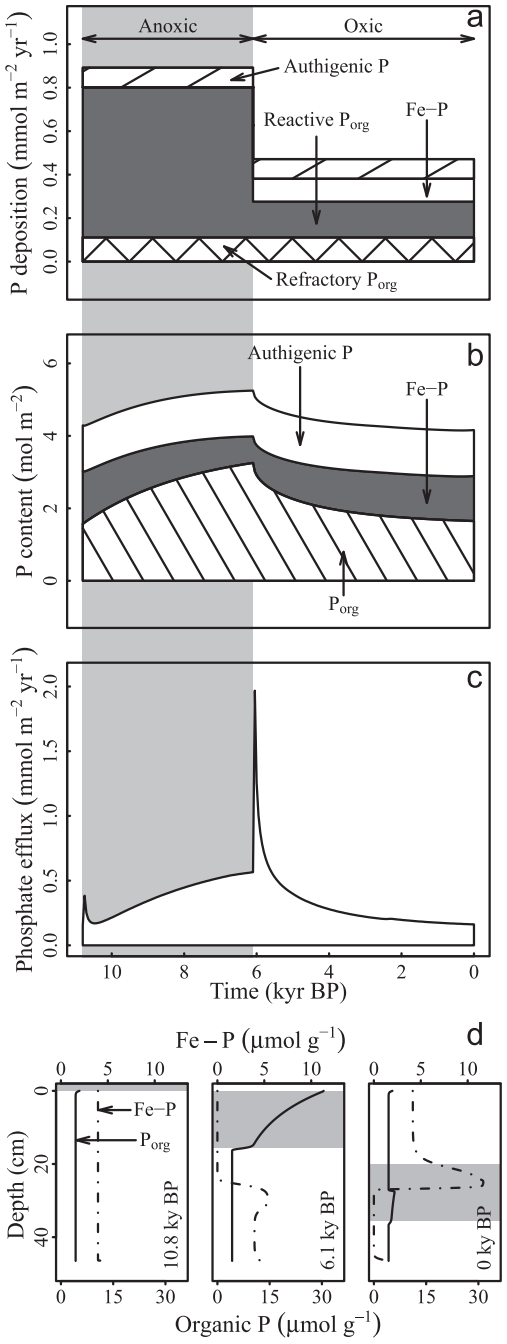

Fig. 7. Sedimentary phosphorus dynamics during the formation and post-depositional alteration of sapropel S1. Panel (a) shows the depositional fluxes of phosphorus during the simulation: reactive and refractory organic phosphorus (P_{org}), iron-bound phosphorus (Fe-P), and authigenic phosphorus. Below, panel (b) plots the depth-integrated phosphorus content of the sediment column and panel (c) shows the benthic phosphate efflux. Profiles of iron-bound phosphorus (dot-dash line) and organic phosphorus (solid line) at 0, 6.1 and 10.8 kyr before present are shown in panel (d).

the reoxygenation of the overlying waters. During the burn-down phase, however, phosphate release is attenuated due to the formation of iron oxyhydroxides that bind phosphate at the redox boundary (Fig. 7d). This iron oxyhydroxide peak is produced mainly by the oxidation of pyrite present within the organic-rich layer. As the pyritic content of the organic-rich layer is a function of water column redox conditions during its formation, sapropels deposited under sulphidic waters are expected to bind more phosphate during burn-down than those deposited under non-sulphidic waters. In sum, sedimentary phosphorus dynamics exhibit a marked redox sensitivity that has the potential to have an impact on basin scale dynamics since sediments are the ultimate phosphorus sink in marine systems (Slomp et al., 2002).

5. CONCLUSIONS

Simulations with a multicomponent diagenetic model demonstrate that the current conceptualisation of sapropel formation and oxidation is quantitatively coherent, describing the dynamics of the system well. Results showed that the depositional flux of reactive organic carbon was elevated during sapropel formation, around three times higher than the present day value, and that the water column was anoxic and sulphidic at that time. Burn-down is dominated by aerobic respiration, the rate of which is an inverse function of time since the bottom waters became oxic once again. A sensitivity analysis of the model revealed that the most important environmental parameters with regard to burn-down are those that regulate the oxidant uptake of the sapropel and the flux of oxygen across the sediment–water interface: namely porosity, bottom oxygen concentration, sedimentation rate and depositional fluxes of organic matter and pyrite during formation. Results demonstrate that all profiles — with the exception of S, $Fe(OH)_3$, Fe-P and $H_2PO_4^-$ — can be replicated when assuming a wide range of redox conditions during sapropel formation. The required depositional flux of organic carbon is a linear function of bottom water oxygen concentration: a higher supply of organic carbon is needed under more oxic conditions to account for increased aerobic respiration. Since anoxia is not needed to achieve the majority of observed geochemical signatures, paleoredox indicators (e.g., C_{org}:S ratio, C_{org}:P_{org} ratio, trace metals) are required to assess the respective roles of oxygen-depletion and primary production in the formation of organic-rich layers in the geological record. Under anoxic conditions, organic carbon is shown to be a direct proxy for export production.

Simulations undertaken to examine nutrient cycling during the formation and oxidation of S1 show that denitrification peaks immediately after reoxygenation of the water column and declines steadily with time. The rate of N_2 production by denitrification is almost 12 times greater than present day and the deposition and preservation of this sapropel has doubled the organic nitrogen content of the upper half metre of the sediment column. The formation and post-depositional alteration of S1 thus represents a substantial nitrogen sink. Phosphorus dynamics also exhibit a marked redox sensitivity. The onset of euxinia produces an initial peak in benthic phosphate efflux due to the reduction of phosphorus-bearing iron oxyhydroxides by hydrogen sulphide diffusing down from the water column. Following this initial pulse, phosphate release from sediments gradually

increases to around 3.5 times the present day value as the organic-rich layer accumulates. Despite enhanced organic phosphorus remineralisation relative to organic carbon, S1 is still enriched in organic phosphorus when deep waters are reventilated and burn-down commences. Consequently, a substantial phosphate pulse is generated, which decreases as an inverse function of time. The efflux of phosphate is attenuated by the formation of iron oxyhydroxides that bind phosphate at the redox boundary. These iron oxyhydroxides are produced chiefly by oxidising sapropelic pyrite. Consequently, sapropels deposited under sulphidic conditions bind phosphate more effectively during burn-down than those formed under non-sulphidic conditions.

ACKNOWLEDGEMENTS

This work was funded by the Netherlands Organisation for Scientific Research (NWO-Vidi to C.P. Slomp). D.C. Reed gratefully acknowledges the hospitality of Dr. B.P. Boudreau at Dalhousie University. We thank three anonymous reviewers for their helpful comments.

APPENDIX A. MULTICOMPONENT MODEL FORMULATION

The general diagenetic equation for a solid species is of the form

$$\frac{\partial C_s}{\partial t} = D_b \frac{\partial^2 C_s}{\partial x^2} + \left(\frac{dD_b}{dx} - v\right)\frac{\partial C_s}{\partial x} + \sum \mathrm{R}_s \qquad \text{(A1)}$$

where C_s is the concentration of the species (μmol L^{-1}; mass per unit volume of solids), t is time (yr), x is distance from the sediment–water interface (cm), D_b is the biodiffusion coefficient ($\mathrm{cm}^2\,\mathrm{yr}^{-1}$), v is the burial velocity ($\mathrm{cm\,yr}^{-1}$), and $\sum \mathrm{R}_s$ is the net reaction rate per unit volume of solids (μmol $\mathrm{L}^{-1}\,\mathrm{yr}^{-1}$) (Berner, 1980; Boudreau, 1997). The preceding equation assumes constant porosity and a depth-dependent biodiffusive mixing defined here as

$$D_b(x) = D_{b0} e^{-\frac{x}{x_b}} \qquad \text{(A2)}$$

where D_{b0} is the biodiffusion coefficient at the sediment–water interface and x_b is the characteristic mixing depth. Similarly, the general diagenetic equation for a solute is

$$\frac{\partial C_p}{\partial t} = \left(D_b + \frac{D'}{\theta^2}\right)\frac{\partial^2 C_p}{\partial x^2} + \left(\frac{dD_b}{dx} - v\right)\frac{\partial C_p}{\partial x} + \sum \mathrm{R}_p \qquad \text{(A3)}$$

where C_p is the concentration of the species (μmol L^{-1}; mass per unit volume of pore water), D' is the appropriate molecular diffusion coefficient adjusted for the considered setting ($\mathrm{cm}^2\,\mathrm{yr}^{-1}$), θ^2 is tortuosity (unitless), and $\sum \mathrm{R}_p$ is the net reaction rate per unit volume of pore water (μmol $\mathrm{L}^{-1}\,\mathrm{yr}^{-1}$) (Berner, 1980; Boudreau, 1997). Tortuosity accounts for particulate material impeding molecular diffusion and is a function of porosity (ϕ) defined here as

Table B1
Primary redox reaction equations. These equations are used to calculate the rate of remineralisation of organic carbon for each oxidation pathway. Eqs. E1–E6 refer to aerobic respiration, denitrification, manganese reduction, iron reduction, sulphate reduction, and methanogenesis, respectively.

$$\mathrm{R}_1 = k_\alpha C_{\mathrm{org}}^{\alpha}\left(\frac{[\mathrm{O_2}]}{k_{\mathrm{O_2}} + [\mathrm{O_2}]}\right) \qquad \text{(E1)}$$

$$\mathrm{R}_2 = k_\alpha C_{\mathrm{org}}^{\alpha}\left(\frac{[\mathrm{NO_3^-}]}{k_{\mathrm{NO_3^-}} + [\mathrm{NO_3^-}]}\right)\left(\frac{k_{\mathrm{O_2}}}{k_{\mathrm{O_2}} + [\mathrm{O_2}]}\right) \qquad \text{(E2)}$$

$$\mathrm{R}_3 = k_\alpha C_{\mathrm{org}}^{\alpha}\left(\frac{[\mathrm{MnO_2}]}{k_{\mathrm{MnO_2}} + [\mathrm{MnO_2}]}\right)\left(\frac{k_{\mathrm{NO_3^-}}}{k_{\mathrm{NO_3^-}} + [\mathrm{NO_3^-}]}\right)\left(\frac{k_{\mathrm{O_2}}}{k_{\mathrm{O_2}} + [\mathrm{O_2}]}\right) \qquad \text{(E3)}$$

$$\mathrm{R}_4 = k_\alpha C_{\mathrm{org}}^{\alpha}\left(\frac{[\mathrm{Fe(OH)_3}]}{k_{\mathrm{Fe(OH)_3}} + [\mathrm{Fe(OH)_3}]}\right)\left(\frac{k_{\mathrm{MnO_2}}}{k_{\mathrm{MnO_2}} + [\mathrm{MnO_2}]}\right)\left(\frac{k_{\mathrm{NO_3^-}}}{k_{\mathrm{NO_3^-}} + [\mathrm{NO_3^-}]}\right)\left(\frac{k_{\mathrm{O_2}}}{k_{\mathrm{O_2}} + [\mathrm{O_2}]}\right) \qquad \text{(E4)}$$

$$\mathrm{R}_5 = \Psi k_\alpha C_{\mathrm{org}}^{\alpha}\left(\frac{[\mathrm{SO_4^{=}}]}{k_{\mathrm{SO_4^{=}}} + [\mathrm{SO_4^{=}}]}\right)\left(\frac{k_{\mathrm{Fe(OH)_3}}}{k_{\mathrm{Fe(OH)_3}} + [\mathrm{Fe(OH)_3}]}\right)\left(\frac{k_{\mathrm{MnO_2}}}{k_{\mathrm{MnO_2}} + [\mathrm{MnO_2}]}\right)\left(\frac{k_{\mathrm{NO_3^-}}}{k_{\mathrm{NO_3^-}} + [\mathrm{NO_3^-}]}\right)\left(\frac{k_{\mathrm{O_2}}}{k_{\mathrm{O_2}} + [\mathrm{O_2}]}\right) \qquad \text{(E5)}$$

$$\mathrm{R}_6 = \Psi k_\alpha C_{\mathrm{org}}^{\alpha}\left(\frac{k_{\mathrm{SO_4^{=}}}}{k_{\mathrm{SO_4^{=}}} + [\mathrm{SO_4^{=}}]}\right)\left(\frac{k_{\mathrm{Fe(OH)_3}}}{k_{\mathrm{Fe(OH)_3}} + [\mathrm{Fe(OH)_3}]}\right)\left(\frac{k_{\mathrm{MnO_2}}}{k_{\mathrm{MnO_2}} + [\mathrm{MnO_2}]}\right)\left(\frac{k_{\mathrm{NO_3^-}}}{k_{\mathrm{NO_3^-}} + [\mathrm{NO_3^-}]}\right)\left(\frac{k_{\mathrm{O_2}}}{k_{\mathrm{O_2}} + [\mathrm{O_2}]}\right) \qquad \text{(E6)}$$

$$\theta^2 = 1 - 2\ln(\phi) \quad \text{(A4)}$$

after Boudreau (1997, p. 132). The behaviour of each chemical species considered by the model is defined by either Eq. (A1) or (A3) with the parameters defined appropriately.

APPENDIX B. REACTION KINETICS

See Tables B1 and B2.

APPENDIX C. CALCULATION OF THE BURN-DOWN DEPTH

To calculate the burn-down depth (BDD) within the model, the proportion of reactive sapropelic organic carbon lost during the oxidation phase is multiplied by the original thickness of the sapropel. For example, if 10% of the reactive organic carbon within the sapropel has been remineralised and the sapropel was 10 cm thick before oxidation, then the BDD is 1 cm. This relies on the upper edge of the organic-rich layer being well-defined and near horizontal, which is evident in both measured and model-generated profiles (i.e., Fig. 1). Indeed, this is the case throughout simulations. Stated mathematically,

$$\mathrm{BDD}(t) = L\left(1 - \frac{\int_{vt}^{vt+L} C^{\alpha}_{\mathrm{org}}(x,t)dx}{\int_{0}^{L} C^{\alpha}_{\mathrm{org}}(x,0)dx}\right) \quad \text{(E21)}$$

In this equation t represents time after the reoxygenation of the bottom waters (yr), x is depth into the sediment with the origin at the sediment–water interface (cm), L is the original thickness of the sapropel (cm), $C^{\alpha}_{\mathrm{org}}(x,t)$ is the reactive organic carbon concentration at location x and time t (μmol L^{-1}; mass per unit volume of solids), and v is the burial rate (cm yr^{-1}). The equation does not differentiate between reactive organic carbon lost by sulphate reduction and other pathways; nonetheless, the rate of sulphate reduction is 3 orders of magnitude smaller than aerobic remineralisation and is, therefore, negligible.

Table B2
Other reaction equations.

$R_7 = k_1[O_2][\Sigma NH_4^+]$	(E7)
$R_8 = k_2[O_2][Mn^{2+}]$	(E8)
$R_9 = k_3[O_2][Fe^{2+}]$	(E9)
$R_{10} = k_4[O_2][FeS]$	(E10)
$R_{11} = k_5[O_2][FeS_2]$	(E11)
$R_{12} = k_6[O_2][\Sigma H_2S]$	(E12)
$R_{13} = k_7[O_2][CH_4]$	(E13)
$R_{14} = k_8[MnO_2][Fe^{2+}]$	(E14)
$R_{15} = k_9[MnO_2][\Sigma H_2S]$	(E15)
$R_{16} = k_{10}[Fe(OH)_3][\Sigma H_2S]$	(E16)
$R_{17} = k_{11}[Fe^{2+}][\Sigma H_2S]$	(E17)
$R_{18} = k_{12}[SO_4^{=}][CH_4]$	(E18)
$R_{19} = k_{13}[S_0]$	(E19)
$R_{20} = k_{14}[FeS][\Sigma H_2S]$	(E20)

REFERENCES

Basso D., Thomson J. and Corselli C. (2004) Indications of low macrobenthic activity in the deep sediments of the eastern Mediterranean Sea. *Sci. Mar.* **68**(Suppl. 3), 53–62.

Berg P., Rysgaard S. and Thamdrup B. (2003) Dynamic modeling of early diagenesis. A case study in an Arctic marine sediment. *Am. J. Sci.* **303**, 905–955.

Berner R. A. (1980) *Early Diagenesis: A Theoretical Approach*. Princeton University Press.

Berner R. A. (1999) Atmospheric oxygen over Phanerozoic time. *Proc. Natl. Acad. Sci. USA* **99**, 10955–10957.

Boudreau B. P. (1986) Mathematics of tracer mixing in sediments: 1. Spatially-dependent, diffusive mixing. *Am. J. Sci.* **286**, 161–198.

Boudreau B. P. (1994) Is burial velocity a master parameter of bioturbation? *Geochim. Cosmochim. Acta* **58**(4), 1243–1249.

Boudreau B. P. (1996) A method-of-lines code for carbon and nutrient diagenesis in aquatic sediments. *Comput. Geosci.* **22**(5), 479–496.

Boudreau B. P. (1997) *Diagenetic Models and Their Implementation: Modelling Transport and Reactions in Aquatic Sediments*. Springer.

Brumsack H.-J. (2006) The trace metal content of recent organic carbon-rich sediments: implications for Cretaceous black shale formation. *Palaeogeogr. Palaeoclimatol. Palaeoecol.* **232**, 344–361.

Burdige D. J. (2006) *Geochemistry of Marine Sediments*. Princeton University Press.

Calvert S. E. and Pedersen T. F. (1993) Geochemistry of recent oxic and anoxic marine sediments: implications for the geological record. *Mar. Geol.* **113**, 67–88.

de Lange G. J., Van Os B., Puysers P. A., Middelburg J. J., Castradori D., Van Santvoort P., Müller P. J., Eggenkamp H. and Prahl F. G. (1994) Possible early diagenetic alteration of palaeo proxies. In *Carbon Cycling in the Glacial Ocean: Constraints on the Ocean's Role in Global Change* (eds. R. Zahn, T. F. Pedersen and M. A. Kaminski). Springer Verlag.

de Lange G. J., Thomson J., Reitz A., Slomp C. P., Principato M. S., Erba E. and Corselli C. (2008) Synchronous basin-wide formation and redox-controlled preservation of a Mediterranean sapropel. *Nat. Geosci.* **1**, 606–610.

Diaz R. J. and Rosenburg R. (2008) Spreading dead zones and consequences for marine ecosystems. *Science* **321**, 926–929.

Dugdale R. C. and Wilkerson F. P. (1988) Nutrient sources and primary productivity in the Eastern Mediterranean. *Oceanol. Acta* **9**, 179–184.

Froelich P. N., Klinkhammer G. P., Bender M. L., Luedtke N. A., Heath G. R., Cullen D., Dauphin P., Hammond D., Hartman B. and Maynard V. (1979) Early oxidation of organic matter in pelagic sediments of the eastern equatorial Atlantic: suboxic diagenesis. *Geochim. Cosmochim. Acta* **43**, 1075–1090.

Goldberg E. D. and Koide M. (1962) Geochronological studies of deep sea sediments by the ionium/thorium method. *Geochim. Cosmochim. Acta* **26**, 417–450.

Guinasso N. L. and Schink D. R. (1975) Quantitative estimates of biological mixing rates in abyssal sediments. *J. Geophys. Res.* **80**(21), 3032–3043.

Hall P. O. J., Brunnegård J., Hulthe G., Martin W. R., Stahl H. and Tengberg A. (2007) Dissolved organic matter in abyssal sediments: core recovery artifacts. *Limnol. Oceanogr.* **52**(1), 19–31.

Holland H. D. (1984) *The Chemical Evolution of the Atmosphere and Oceans*. Princeton University Press.

Ingall E. D. and Jahnke R. (1994) Evidence for enhanced phosphorus regeneration from marine sediments overlain by oxygen depleted waters. *Geochim. Cosmochim. Acta* **58**(11), 2571–2575.

Ingall E. D., Bustin R. M. and Van Cappellen P. (1993) Influence of water column anoxia on the burial and preservation of carbon and phosphorus in marine shales. *Geochim. Cosmochim. Acta* **57**, 303–316.

Jung M., Ilmberger J., Mangini A. and Emeis K.-C. (1997) Why some Mediterranean sapropels survived burn-down (and others did not). *Mar. Geol.* **141**, 51–60.

Kidd R. B., Cita M. B. and Ryan W. B. F. (1978) Stratigraphy of eastern Mediterranean sapropel sequences recovered during DSDP Leg42A and their paleoenvironmental significance. *Init. Rep. Deep Sea Drilling Proj.* **42A**, 421–443.

Kraal P., Slomp C. P. and de Lange G. J. (2010a) Sedimentary organic carbon to phosphorus ratios as a redox proxy in Quaternary records from the Mediterranean. *Chem. Geol.* **277**(1–2), 167–177.

Kraal P., Slomp C. P., Forster A. and Kuypers M. M. M. (2010b) Phosphorus cycling from the margin to abyssal depths in the proto-Atlantic during oceanic anoxic event 2. *Palaeogeogr. Palaeoclimatol. Palaeoecol.* **295**, 42–54.

Krom M. D., Kress N., Brenner S. and Gordon L. I. (1991) Phosphorus limitation of primary productivity in the eastern Mediterranean Sea. *Limnol. Oceanogr.* **36**(3), 424–432.

Krom M. D., Herut B. and Mantoura R. F. C. (2004) Nutrient budget for the Eastern Mediterranean: implications for phosphorus limitation. *Limnol. Oceanogr.* **49**(5), 1582–1592.

Kurganov A. and Tadmor E. (2000) New high-resolution central schemes for nonlinear conservation laws and convection–diffusion equations. *J. Comput. Phys.* **160**, 241–282.

Leventhal J. S. (1995) Carbon–sulfur plots to show diagenetic and epigenetic sulfidation in sediments. *Geochim. Cosmochim. Acta* **59**(6), 1207–1211.

Mangini A., Eisenhauer A. and Walter P. (1991) A spike of CO_2 in the atmosphere at glacial–interglacial boundaries induced by rapid deposition of manganese in the oceans. *Tellus B* **43**, 97–105.

Moodley L., Middelburg J. J., Herman P. M. J., Soetaert K. and de Lange G. J. (2005) Oxygenation and organic-matter preservation in marine sediments: direct experimental evidence from ancient organic carbon-rich deposits. *Geology* **33**(11), 889–892.

Passier H. F., Middelburg J. J., van Os B. J. H. and de Lange G. J. (1996) Diagenetic pyritisation under eastern Mediterranean sapropels caused by downward sulphide diffusion. *Geochim. Cosmochim. Acta* **60**(5), 751–763.

Passier H. F., Middelburg J. J., de Lange G. J. and Böttcher M. E. (1999) Modes of sapropel formation in the eastern Mediterranean: some constraints based on pyrite properties. *Mar. Geol.* **153**, 199–219.

Passier H. F., de Lange G. J. and Dekkers M. J. (2001) Magnetic properties and geochemistry of the active oxidation front and the youngest sapropel in the eastern Mediterranean Sea. *Geophys. J. Int.* **145**, 604–614.

Pruysers P. A., de Lange G. J., Middelburg J. J. and Hydes D. J. (1993) The diagenetic formation of metal-rich layers in sapropel-containing sediments in the eastern Mediterranean. *Geochim. Cosmochim. Acta* **57**, 527–536.

R Development Core Team (2006) *R: A Language and Environment for Statistical Computing*. R Foundation for Statistical Computing, Vienna, Austria. ISBN: 3-900051-07-0.

Reitz A., Thomson J., de Lange G. J. and Hensen C. (2006) Source and development of large manganese enrichments above eastern Mediterranean sapropel S1. *Paleoceanography* **21**(PA3007).

Richter R. (1952) Fluidal-texture in Sediment-Gesteinen und ober Sedifluktion berhaupt. *Notizbl Hess Landesamtes Bodenforsch Wiesbaden* **3**, 67–81.

Rickard D. (1997) Kinetics of pyrite formation by the H_2S oxidation of iron(II) monosulfide in aqueous solutions between 25 and 125 °C: the rate equation. *Geochim. Cosmochim. Acta* **61**, 115–134.

Rohling E. J. and Hilgen F. J. (1991) The Eastern Mediterranean climate at times of sapropel formation: a review. *Geol. Mijnbouw* **70**, 253–264.

Slomp C. P., Epping E. H. G., Helder W. and Van Raaphorst W. (1996) A key role for iron-bound phosphorus in authigenic apatite formation in North Atlantic continental platform sediments. *J. Mar. Res.* **54**, 1179–1205.

Slomp C. P., Thomson J. and de Lange G. J. (2002) Enhanced regeneration of phosphorus during formation of the most recent eastern Mediterranean sapropel (S1). *Geochim. Cosmochim. Acta* **66**(7), 1171–1184.

Slomp C. P., Thomson J. and de Lange G. J. (2004) Controls on phosphorus regeneration and burial during formation of eastern Mediterranean sapropels. *Mar. Geol.* **203**, 141–159.

Soetaert K. and Herman P. M. J. (2009) *A Practical Guide to Ecological Modelling: Using R as a Simulation Platform*. Springer.

Soetaert K., Petzoldt T. and Setzer R. W. (2010) Solving differential equations in R: package deSolve. *J. Stat. Softw.* **33**(9), 1–25.

Suess E. (1980) Particulate organic carbon flux in the oceans — surface productivity and oxygen utilization. *Nature* **288**, 260–263.

Thomson J., Mercone D., de Lange G. J. and Van Santvoort P. J. M. (1999) Review of recent advances in the interpretation of eastern Mediterranean sapropel S1 from geochemical evidence. *Mar. Geol.* **153**, 77–89.

Tromp T. K., Van Cappellen P. and Key R. M. (1995) A global model for the early diagenesis of organic carbon and organic phosphorus in marine sediments. *Geochim. Cosmochim. Acta* **59**(7), 1259–1284.

Van Cappellen P. and Wang Y. (1995) Metal cycling in surface sediments: modeling the interplay of transport and reaction. In *Metal Contaminated Sediments* (ed. H. E. Allen). Ann Arbor Press.

Van Santvoort P. J. M., de Lange G. J., Thomson J., Cussen H., Wilson T. R. S., Krom M. D. and Ströhle K. (1996) Active post-depositional oxidation of the most recent sapropel (S1) in sediments of the eastern Mediterranean Sea. *Geochim. Cosmochim. Acta* **60**(21), 4007–4024.

Van Santvoort P. J. M., de Lange G. J., Thomson J., Colley S., Meysman F. J. R. and Slomp C. P. (2002) Oxidation and origin of organic matter in surficial eastern Mediterranean hemipelagic sediments. *Aquat. Geochem.* **8**, 153–175.

Wang Y. and Van Cappellen P. (1996) A multicomponent reactive transport model of early diagenesis: application to redox cycling in coastal marine sediments. *Geochim. Cosmochim. Acta* **60**, 2993–3014.

Associate editor: David J. Burdige